Int. J. Electrochem. Sci., 15 **(2020)** 3242 – 3254, doi: 10.20964/2020.04.46

International Journal of
ELECTROCHEMICAL
SCIENCE
www.electrochemsci.org

Study on the Electrocatalytic Performance of Porous Conductive Materials Based on an In Situ Growth of Bimetal Phosphides with Plasma

Mojie sun[1], *Bixue Gao*[1], *Shijie Wang*[1], *Chi Wang*[1], *Dongyao Lin*[3], *Xiaochen Song*[2,*], *Zhao Wang*[1,*]

[1] School of Chemical Engineering, Northeast Electric Power University, 169# Changchun Road, Chuanying District, Jilin 132012, China
[2] School of Mechanical Engineering, Northeast Electric Power University, 169# Changchun Road, Chuanying District, Jilin 132012, China
[3] School of Energy and Power Engineering, Northeast Electric Power University, 169# Changchun Road, Chuanying District, Jilin 132012, China
[*]E-mail: songxiaochen0306@163.com

Received: 8 December 2019 / *Accepted:* 27 January 2020 / *Published:* 10 March 2020

To find alternative solutions for the high cost of noble metals in the process of electrocatalytic hydrogen evolution, a hydrothermal method was used to in situ grow a precursor material with nanosheet (100 nm) and nanorod (100 nm) micromorphologies on the surface of a Ni foam (NF). Subsequently, phosphorylation was performed on the precursor surface by a plasma-enhanced chemical vapor deposition (PECVD) method to obtain a nickel-cobalt double metal phosphide with a needle-like nanoarray morphology. NiCoP-PECVD has a simple preparation method and a regular morphology, and it has excellent HER performance over a large pH range as evidenced from electrochemical tests. When the current density is 10 $mA \cdot cm^{-2}$, the hydrogen evolution overpotentials in the acidic solution (0.5 M H_2SO_4) and alkaline solution (1 M KOH) are 78 mV and 80 mV, respectively. Compared with Ni_2P-PECVD and NiCoP-CVD, the above values are significant lower. The chronopotential (CP) test showed that the material has good HER stability over 12 h. The ECSA test results show that both the Co doping and the PECVD method can help to increase the number of active sites of the material and improve its electrocatalytic activity. The above results are favorable for designing and developing low-cost, high-efficiency transition metal phosphorus catalysts.

Keywords: PECVD; HER; Double metal phosphide; Acicular nanoarray; Double microtopography

1. INTRODUCTION

With the progress of industry and the development of society, people's demand for energy is increasing, and the rapid consumption of fossil fuel energy and its contribution toward environmental pollution have gradually become more prominent[1-3]. Therefore, research and development of green

and efficient clean energy are urgent. Hydrogen energy, as a clean and renewable secondary energy source, meets the needs of energy development and the environment and is an ideal substitute for fossil fuels. Therefore, hydrogen energy will occupy a very important position in future energy structures[4-7].

If hydrogen replaces fossil energy, it must be capable of large-scale industrial production[8]. Hydrogen in nature generally exists in water and carbohydrates. As the demand for hydrogen energy increases, it is imperative to use efficient, clean, and energy-saving means of hydrogen production. Researchers have developed many methods for producing hydrogen, such as partially oxidizing hydrocarbons[9], electrolyzing water[10-12], and photolyzing water[13]; additionally, biological hydrogen production[14], molten salt electrolysis[15], methanol cracking[16], and organic solvent decomposition have also been demonstrated. Hydrogen produced from electrolyzed water is an ideal method for hydrogen production due to its high efficiency and environmental friendliness; additionally, there is an abundance of raw materials[17]. During the electrolysis process, hydrogen and oxygen are generated simultaneously at the cathode and anode through electrolysis. The two half reactions are the oxygen evolution reaction (OER) of the anode[18] and the hydrogen evolution reaction (HER) of the cathode[19], both of which determine the efficiency of electrolyzed water. Therefore, the use of electrocatalysts with good performance has become a main research direction. Among the known electrocatalysts, noble metals have the best electrocatalytic performance (for example, Pt in the HER reaction and IrO2 in the OER reaction)[20,21]. However, the high cost and scarcity of precious metals are the main factors limiting their development[22]. Thus, researchers have explored transition metals with an abundance of resources (Ni, Co, Mo, Fe, V, etc.), with the goal to replace precious metal catalysts with novel compounds (hydroxides, sulfides, oxides, phosphides, etc.) [23 -28].

A transition metal phosphide (TMP) has a catalytic mechanism similar to hydrogenase, which makes its catalytic activity relatively high and has attracted widespread attention from researchers[29,30]. However, TMP has lower catalytic performance than that of noble metal electrodes. Studies have shown that increasing the specific surface area, conductivity, and number of active sites of the catalyst can effectively improve the electrocatalytic performance[31]. Metal doping can effectively improve the conductivity of the catalyst and improve its electrocatalytic performance[32]. Correspondingly, compared with a single metal phosphide, a double metal phosphide usually exhibits more valence changes and better activity[33]. As a new catalyst for the HER reaction, literature related to NiCoP[34-37] has appeared in large numbers in recent years.

In this experiment, a precursor (NiO-CoO) with two nanowire array morphologies is grown in situ on the surface of an NF skeleton by a hydrothermal method. A PECVD[38,39] method is used to phosphorylate the surface to form a double metal phosphide, and thus, an electrocatalyst (NiCoP) with excellent HER performance is obtained.

2. EXPERIMENTS

2.1 Materials

Cobalt nitrate ($Co(NO_3)_2 \cdot 6H_2O$, AR, Shanghai Aladdin Biochemical Technology Co., Ltd.,

China), Ni foam (NF, Huirui wire mesh factory, China), sodium hypophosphite (NaH_2PO_2, AR, Shanghai Aladdin Biochemical Technology Co., Ltd., China), hydrochloric acid (HCl, AR, Xilong Chemical Co., Ltd., China), sulfuric acid (H_2SO_4, AR, Beijing Chemical Plant, China), potassium hydroxide (KOH, GR, Tianjin Fuchen Chemical Reagent Factory, China), acetone (CH_3COCH_3, AR, Yantai Shuangshuang Chemical Co., Ltd., China), and absolute ethanol (C_2H_6O, AR, Tianjin Fengchuan Chemical Reagent Technology Co., Ltd., China) were obtained and used in this experiment.

2.2 Preparation of Ni_2P/NF

The experimental scheme is shown in Figure 1:

(1) The NF was cut into 2×3 cm samples and then subsequently placed in 3 M HCl, acetone, absolute ethanol, and ultrapure water for 15 min of ultrasonic cleaning. Then, the sample was removed and placed under vacuum for 6 h.

(2) Cobalt nitrate (1.746 g) and 1.2 g of urea were weighed and dissolved in 40 mL of ultrapure water. Then, the solution was magnetically stirred for 10 min. Next, the pretreated NF and solution were placed into a 50-mL reaction kettle at the same time and then sonicated for 2 h. Subsequently, a hydrothermal reaction was performed at 130°C for 12 h, and then the hydrothermal reaction product was vacuum dried to obtain a precursor (pink).

(3) The precursor was placed in a porcelain boat filled with 2.5 g of sodium hypophosphite, and then PECVD was conducted. Under an argon atmosphere, the temperature was raised to 250°C at 3°C·min^{-1} for 1 h. When the temperature rose to 250°C, the plasma was enhanced for 1 h at 80 W. The prepared product was ultrasonically cleaned for 5 min and then vacuum-dried to obtain a black sheet-like NiCoP/NF.

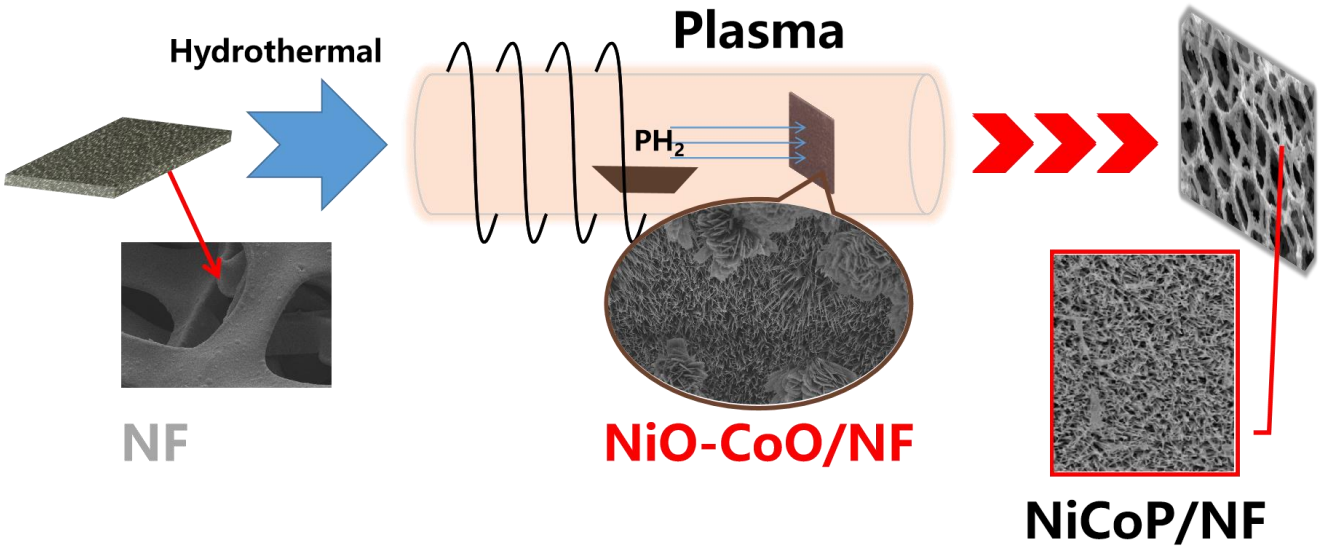

Figure 1. NiCoP synthesis scheme.

2.3 Electrochemical analysis method

In this experiment, a three-electrode system was used to electrochemically test the prepared nickel-based hydrogen evolution material through an electrochemical workstation. With a scanning rate

of 5 $mV \cdot s^{-1}$, a linear sweep voltammetry (LSV) method was used to test the hydrogen evolution overpotential. A constant current density of 10 $mA \cdot cm^{-2}$ was used to test the chronopotentiometry (CP) of the catalyst over 12 h. A CV test was performed at different scanning rates (10 $mV \cdot s^{-1}$, 20 $mV \cdot s^{-1}$, 40 $mV \cdot s^{-1}$, 60 $mV \cdot s^{-1}$, 80 $mV \cdot s^{-1}$, 100 $mV \cdot s^{-1}$, and 120 $mV \cdot s^{-1}$) in an area where no redox occurred. By calculating the electric double layer capacitance (C_{dl}), the electrochemical surface area (ECSA) of the catalyst was calculated. The electrolytes used in the electrochemical tests were 0.5 M H_2SO_4 and 1 M KOH solutions, which represented acidic and alkaline media, respectively. In the three-electrode system, the nickel-based hydrogen evolution material synthesized in this experiment was used as the working electrode (WE), and a graphite sheet was used as the counter electrode (CE). A saturated calomel electrode (SCE) was used as a reference electrode (RE) in the acidic medium, and a mercury oxide mercury electrode (Hg/HgO) was used as the RE in the alkaline medium. The data obtained from the tests, E_{SCE} or $E_{Hg/HgO}$, were converted into E_{RHE} at the reversible hydrogen electrode potential by formulas (1) and (2):

$$E_{RHE}=E_{SCE}+0.244+0.0591pH \quad (1)$$

$$E_{RHE}=E_{Hg/HgO}+0.098+0.0591pH \quad (2)$$

A Tafel curve is drawn by taking a logarithm of the current density in the LSV curve as the independent variable and the hydrogen evolution potential as the dependent variable. This curve can reflect the change in the hydrogen overpotential of the material when the current density increases to a power of 10 as the base. On this basis, the Tafel slope b is determined according to the Tafel formula (formula (3)) and its deformation formula (formula (4)):

$$\eta=a+b\cdot\log|j| \quad (3)$$

$$b=\frac{\eta_2-\eta_1}{\log|j|_2-\log|j|_1}=\frac{\Delta\eta}{\Delta\lg|j|} \quad (4)$$

Where b is the Tafel slope, a is the transfer coefficient, j is the current density, and η is the hydrogen evolution overpotential of the electrode, which are all important parameters that characterize the nature of the electrode and its reaction. The values of a and b are related to the electrode reaction mechanism, and j is related to the electrode material. The value of j can indicate the level of catalytic activity of the electrode. The higher the value of j is, the greater the catalytic activity of the electrode reaction. The effect of the electrode potential on the electrochemical reaction speed is mainly achieved by affecting the activation energy of the reaction, so the electrode reaction speed can be reflected by the magnitude of the electrode reaction activation energy at different potentials.

3. RESULTS AND DISCUSSION

3.1 Structural and morphology characterization

Figure 2 shows the comparison of XRD spectra of NF before and after the hydrothermal and PECVD reactions. It can be seen from Figure 2a that after the hydrothermal reaction, the XRD spectrum of the material maintains the characteristic peaks of Ni, and new characteristic peaks are generated, at positions of 37°, 43°, 62°, 75°, 79°. A comparison with JADE software shows that these five characteristic peaks correspond to the (111), (200), (220), (311), and (222) crystal planes of NiO and are

consistent with the NiO standard card JCPDS#73-1523. Additionally, more obvious characteristic peaks appear at 34°, 40°, 57°, 68°, and 72°. The above characteristic peaks are consistent with the CoO standard card JCPDS#42-1300. The remaining three characteristic peaks are characteristic peaks of elemental Ni. After an XRD characterization, it can be determined that NiO and CoO are grown in situ on the surface of nickel foam. According to the analysis of Figure 2b, after the PECVD reaction of the precursor, the characteristic peaks of the material appear at 2θ= 30°, 32°, 41°, 45°, 47°, 54°, 55°, 61°, 64°, 66°, 70°, 73°, 75°, which are characteristic peaks that correspond to the (110), (101), (111), (201), (210), (300), (211), (301), (112), (310), (221) and (311) crystal planes of NiCoP (JCPDS#71-2336). The above results show that the PECVD method can promote the phosphorylation of the precursor and grow NiCoP in situ on the NF surface.

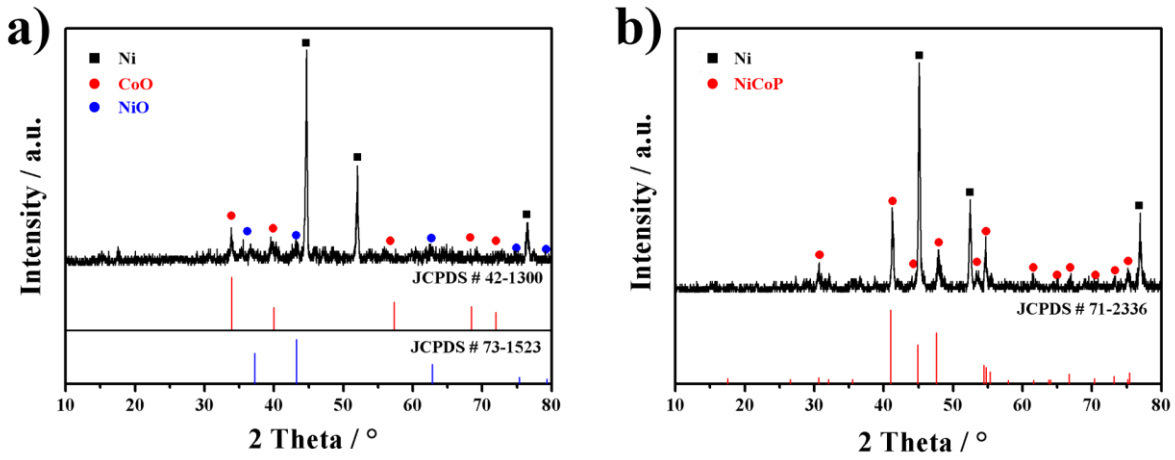

Figure 2. XRD spectrum of the a) precursor and b) NiCoP/NF.

Figure 3 is an SEM comparison image of NF before and after the hydrothermal and PECVD reactions. Figures 3a, 3c, and 3g are high-magnification SEM images of the NF, precursor, and NiCoP/NF. Comparing these three images, we can see that the skeleton width of the NF before and after the reaction is 60, 80, and 90 μm. Moreover, the surface of the NF before the reaction is relatively smooth. Increasing the width of the skeleton and making the surface rougher help to increase the specific surface area of the material. Figure 3d is a high-magnification SEM image of the precursor. The surface of the precursor has two nanomaterials with a "flower-like" morphology. The red and green parts in 3d are enlarged to obtain Figure 3e and 3f. It is found that the materials grown on the surface of nickel foam are "needle-like" nanorods with a diameter of approximately 50 nm and "zigzag" nanosheets with a thickness of approximately 50 nm. Figures 3h and 3i are high-magnification SEM images of NiCoP/NF. It can be seen from the figures that after the precursor undergoes PECVD, the "flower-like" nanomaterials on the surface of the material are nanoarrays composed of nanorods with a diameter of 70 nm. Its unique microscopic morphology is conducive to increasing the specific surface area of the material, thereby increasing the possibility of active site exposure.

As shown in Figure 4, Figure 4a shows the results of the EDS test of the precursor. The results show that after the hydrothermal reaction, the material formed on the nickel foam surface contains Ni, Co, O, and C. According to the table in Figure 4a, the weight percentages (wt%) of Ni, Co, and O are 11.41, 34.68, and 43.10, respectively, and the atomic percentages (at%) are 5.63, 13.04, and 59.69,

respectively, where the C comes from the test carrier. As shown in Figure 4b, the results show that after the precursor undergoes the PECVD reaction, the material formed on the nickel foam surface contains the elements Ni, Co, P, O, and C. The table in the figure shows that the weight percentages (wt%) of Ni, Co, and P are 17.75, 15.74, and 19.29, respectively, and the atomic percentages (at%) are 10.26, 8.52, and 14.19, respectively. Combined with the XRD characterization results, it can be seen that the Ni, Co, and P on the surface are derived from the NiCoP nanoarray and the base material (NF), and the O element is derived from the incompletely reacted NiO, CoO, and the oxidation formed on the surface during storage.

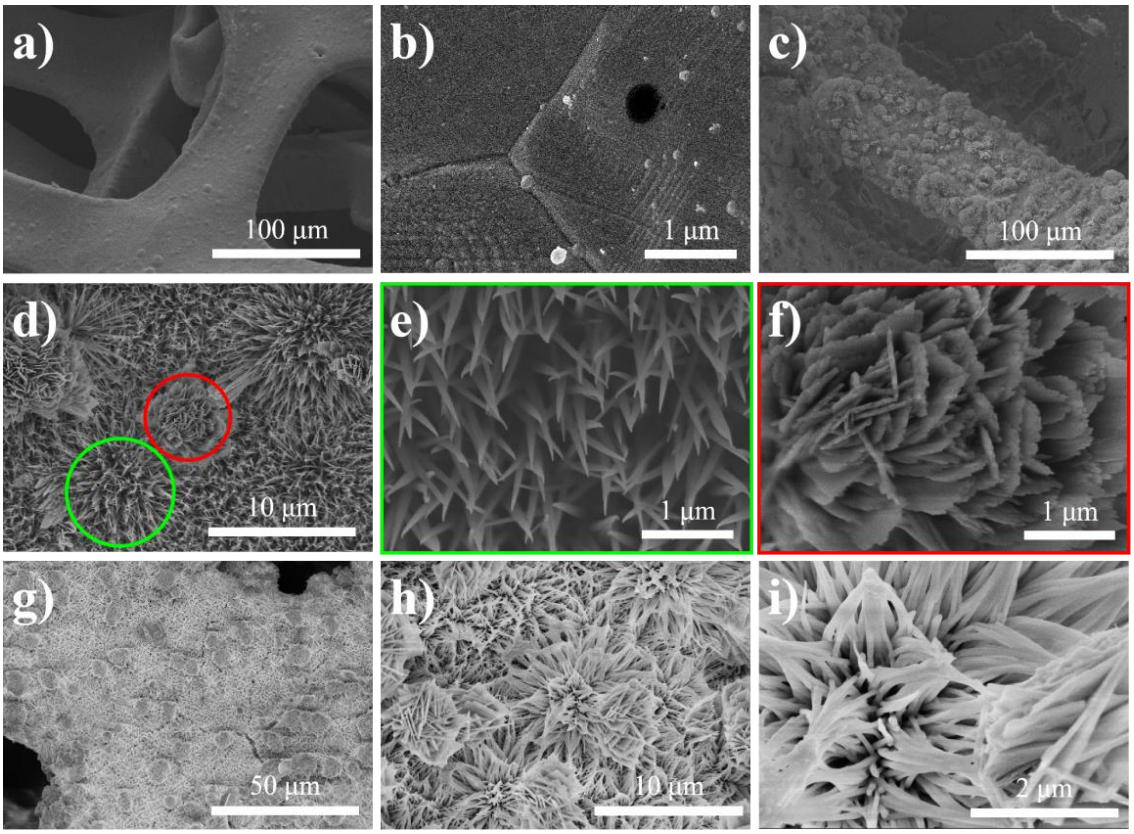

Figure 3. SEM images of the a-b) NF, c-f) precursor, and g-i) NiCoP/NF.

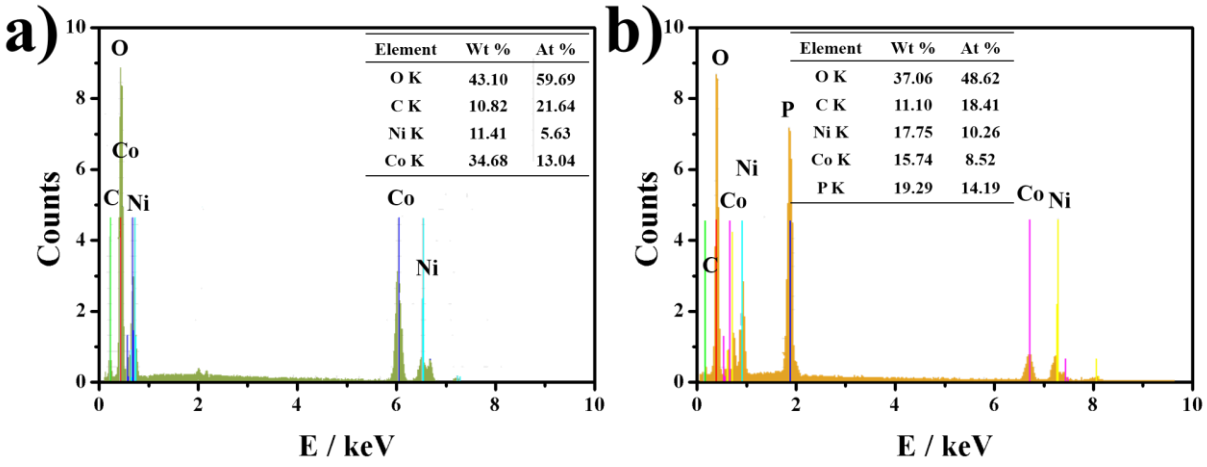

Figure 4. EDS test results of the a) precursor and b) NiCoP/NF.

To further determine the composition of the material and the elemental valence of the active material, we performed an XPS characterization of the material. Figure 5a is the XPS full spectrum of NiCoP/NF. It can be seen from the figure that the tested sample contains four elements: C, Co, P, and Ni, which is consistent with the abovementioned EDS results.

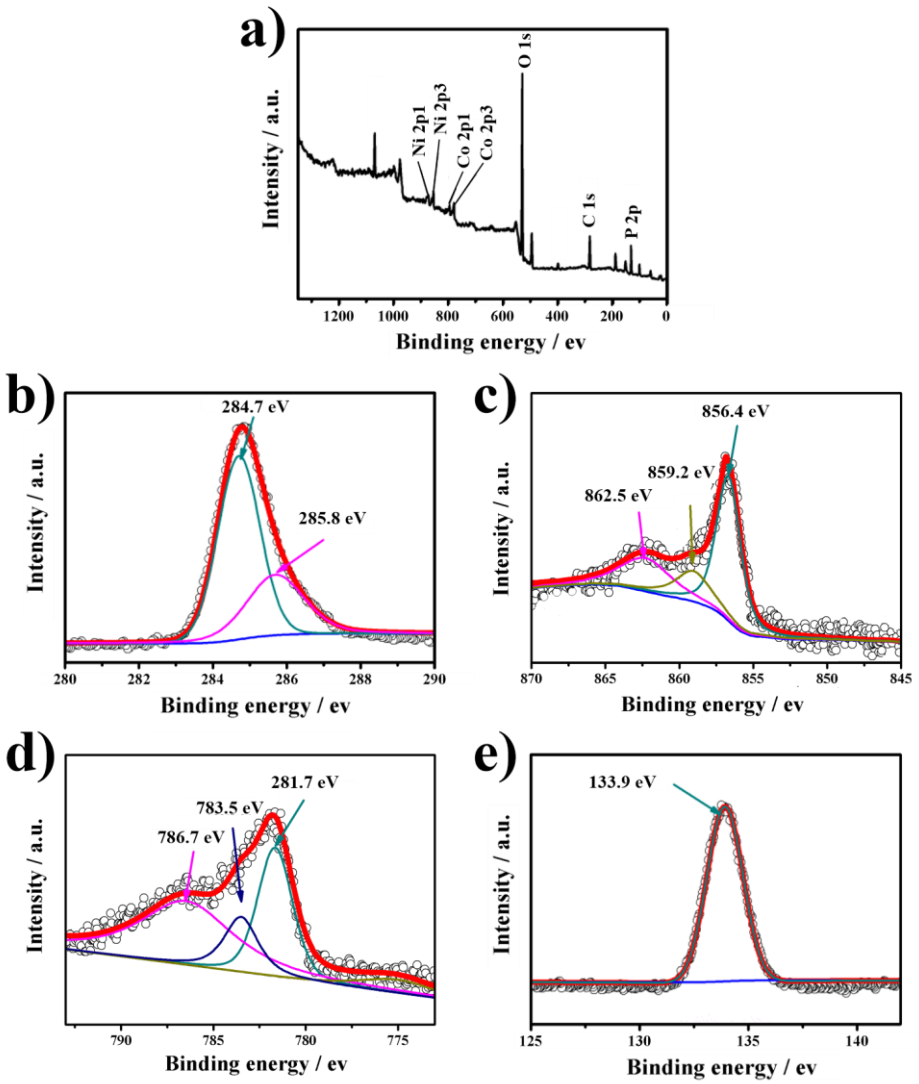

Figure 5. XPS test results of the following: a) survey spectrum, b) C 1s spectra, c) Ni 2p spectra, d) Co 2p spectra, and e) P 2p spectra.

To further analyze the existence states and elemental bonds in NiCoP/NF, a fine spectrum analysis was performed for C, Co, P and Ni. Figure 5b shows a fine spectrum for C 1s. After consulting the binding energy table of C, it can be found that there are two forms of C on the NiCoP/NF surface. The characteristic peaks when the binding energies are 284.6 eV and 285 eV are C-C and C=C, respectively [40]. Figure 5c shows the fine spectrum of Ni 2p. Peak fitting is performed, and it can be seen that Ni on the NiCoP/NF surface exists in two forms. The characteristic peaks of 856.4 eV, 859.2 eV, and 862.5 eV are consistent with those of Ni-P and Ni-POx[41,42]. Figure 5d shows the fine

spectrum of Co 2p, which is fitted to the peaks. Three characteristic Co peaks appear on the surface of NiCoP/NF at binding energies of 781.7 eV, 783.5 eV, and 786.7 eV. The characteristic peak at 781.7 eV is related to the Co oxidation state of Co-PO_x [43]. The other two characteristic peaks are consistent with Co-P [44]. Figure 5e shows a fitting curve of P 2p. A characteristic peak appears at a binding energy of 135.0 eV, which indicates that the P 2p binding energy is smaller than the P 2p binding energy of the element P (135.0 eV), which indicates that the P substance in NiCoP has a very small negative charge ($P^{\delta-}$, $0 < \delta < 1$). It can therefore be concluded that there is an electron transfer from Ni to P [45] and that the small charge mainly indicates a covalent feature with a small ion contribution.

3.2 Electrocatalytic HER properties of NiCoP/NF

In this part of the experiment, a three-electrode system is used to test the electrochemical performance of NiCoP/NF electrodes prepared by PECVD in an acidic solution (0.5 M H_2SO_4) and an alkaline solution (1 M KOH). As a control test, we tested unreacted NF, Ni_2P/NF prepared by PECVD, and NiCoP/NF prepared by chemical vapor deposition. They are named NiCoP-PECVD, NF, Ni_2P-PECVD and NiCoP-CVD.

The electrochemical performance of NiCoP-PECVD in acidic media is shown in Figure 6. Figure 6a shows the LSV curves of different materials in the 0.5 M H_2SO_4 solution. It can be seen from the figure that NiCoP-PECVD has a hydrogen evolution overpotential of 78 mV at a current density of 10 $mA \cdot cm^{-2}$; when the overpotential reaches 209 mV, its current density is 100 $mA \cdot cm^{-2}$. The hydrogen evolution overpotential is significantly reduced compared to those of the single metal phosphide (Ni_2P-PECVD) prepared by PECVD and the double metal phosphide (NiCoP-CVD) prepared by CVD. Figure 6b is the Tafel curve corresponding to Figure 6a. According to the Tafel formula, the Tafel slope (63 $mV \cdot dec^{-1}$) of NiCoP-PECVD is also significantly reduced compared with those of the other three materials. This result indicates that NiCoP-PECVD has the fastest reaction kinetics.

We evaluated the stability of hyperbranched electrodes through an overpotential time measurement and a CV test at 50 $mV \cdot s^{-1}$. As shown by the e-t curve in Figure 6c, in the 12-hour CP test of NiCoP-PECVD, the overpotential change is only approximately 15 mV.

Therefore, NiCoP-PECVD has relatively good stability in the 0.5 M H_2SO_4 solution. At the same time, the LSV curves of the material almost overlapped after a 2000-cycle CV scan, thus demonstrating the durability of NiCoP-PECVD. To further reveal why NiCoP-PECVD has high electrochemical activity, the electric double layer capacitance (C_{dl}) of NiCoP-PECVD was calculated using the CV curves at different sweep speeds in 0.5 M H_2SO_4 solution. The Cdl can accurately evaluate the electrochemical active area (ECSA) of the material. Figure 7d shows the linear relationship between the difference in current density and the scan rate. It can be seen from the slope calculation that the C_{dl} of NiCoP-PECVD in 0.5 M H_2SO_4 is 65.5 $mF \cdot cm^{-2}$. After comparison, it can be seen that the PECVD method and the Co doping can effectively improve the electrochemically active surface area of the material.

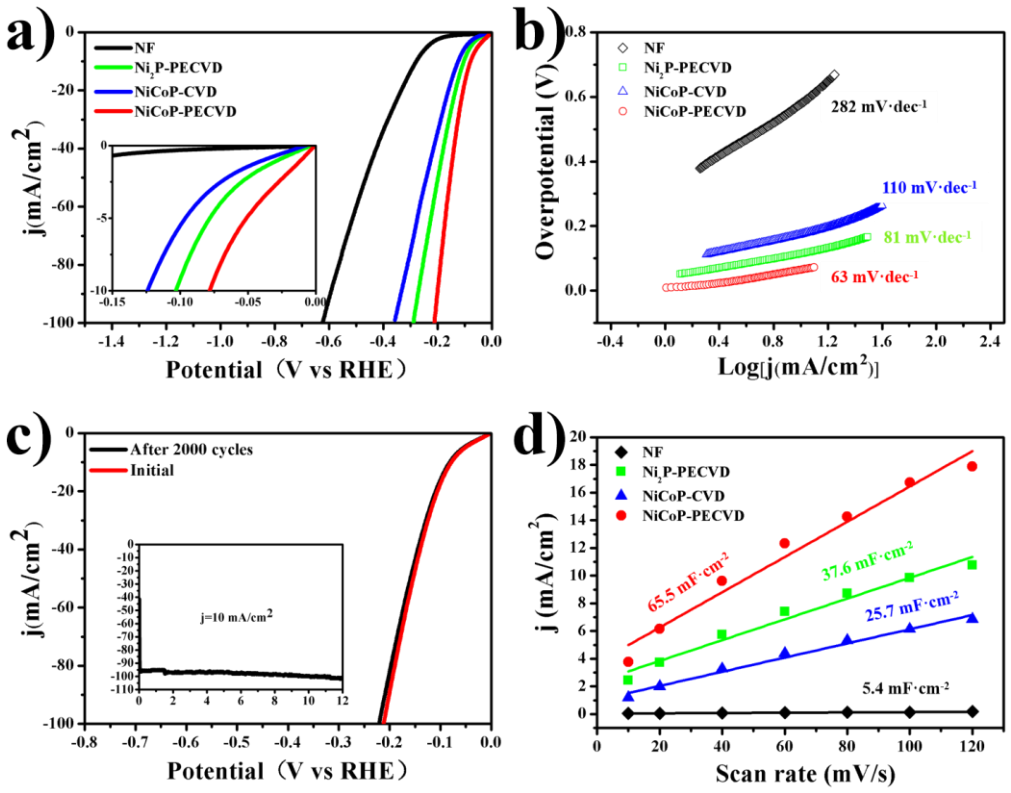

Figure 6. Electrochemical test results in the 0.5 M H_2SO_4 solution: a) LSV curve, b) Tafel curve, and c) LSV curve after 2000 CV cycles; the inset is the e-t curve. d) Linear relationship between the different scan rates (10~120 $mV \cdot s^{-1}$) and current densities to determine the Cdl for ECSA.

Table 1. Comparison of the catalytic parameters of different HER catalysts in 0.5 M H_2SO_4

Catalyst	η (mV) at J = 10 mA cm^{-2}	Tafel slope ($mV \cdot dec^{-1}$)	ECSA ($mF \cdot cm^{-2}$)	Reference
NiCoP/NF-PECVD	78	63	65.5	This work
NiCoP/NF-CVD	108	81	37.6	This work
CoP_3/Ni2P	115	31	38.5	[46]
Ni_2P/NiCoP@NCCs	120	79	8	[47]
Ni_2P/NiCoP@NHCCs	136	90	7	[47]
CoP Hollow	159	59	--	[48]
CoP-CNTs	139	52	--	[49]
Ni_2P Ps-3	158	73	35	[50]
CoP-12/GA	121	50	20.1	[51]

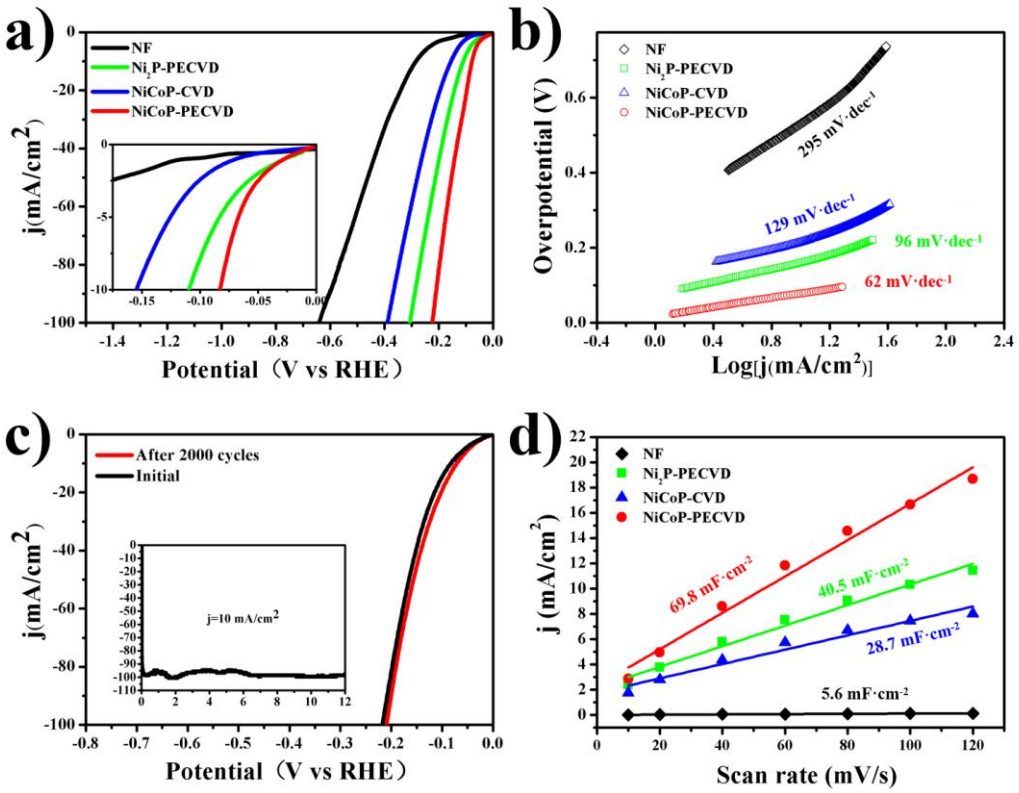

Figure 7. Electrochemical test results in the 1 M KOH solution: a) LSV curve, b) Tafel curve, and c) LSV curve after 2000 CV cycles; the inset is the e-t curve. d) Linear relationship between the different scan rates (10~120 mV·s^{-1}) and current densities to determine the Cdl for ECSA.

Figure 7a is the LSV curve of the material in 1 M KOH. The current density of NiCoP-PECVD reaches 10 and 100 mA·cm-^{2} at overpotentials of 80 and 214 mV, respectively. NiCoP-CVD and Ni_2P-PECVD can only be achieved when the overpotential reaches 154 and 110 mV (η=10 mA·cm^{-2}).

Therefore, NiCoP-PECVD has an extremely low initial hydrogen evolution overpotential in the alkaline media, which can effectively save power and energy during the process of producing hydrogen by electrolyzing water. Figure 7b is the corresponding Tafel curve of NiCoP-PECVD in 1 M KOH. The linear fitting shows that the Tafel slope of NiCoP-PECVD is 62 mV·dec^{-1}, which is lower than the Tafel slopes of NiCoP-CVD and Ni_2P-PECVD. The above also indicates that as the potential increases, the rate of electrochemical hydrogen evolution increases rapidly; thus, fast electrocatalysis kinetics are observed. Figure 8c is a comparison of the e-t curve obtained after the 12 h CP test of NiCoP-PECVD and the LSV curve obtained after 2000 cycles of CV. By comparison, NiCoP-PECVD has a relatively stable hydrogen evolution overpotential in alkaline electrolytes. Moreover, the ECSA of different materials was tested. The results are shown in Figure 7d. NiCoP-PECVD has the highest ECSA (C_{dl} = 69.8 mF·cm^{-2}) in 1 M KOH, which is better than those of NiCoP-CVD (C_{dl} = 28.7 mF·cm^{-2}) and Ni_2P-PECVD (C_{dl} = 69.8 mF·cm^{-2}). The high catalytic active surface area can reasonably be attributed to the PECVD method, and the metal doping can effectively promote exposure and increase the number of active sites.

According to the comparison of the data in Tables 1 and 2, the NiCoP-PECVD prepared in this

experiment has a relatively low hydrogen evolution overpotential in 0.5 M H_2SO_4 and 1 M KOH. By comparing the ECSA data, we know that the materials prepared by the PECVD method can expose more active sites, which then promote the electrocatalytic reaction. At the same time, using NF as a substrate can increase the specific surface area of the material and accelerate the desorption of hydrogen on the electrode surface.

Table 2. Comparison of the catalytic parameters of different HER catalysts in 1 M KOH

Catalyst	η (mV) at J = 10 mA cm^{-2}	Tafel slope ($mV \cdot dec^{-1}$)	ECSA ($mF \cdot cm^{-2}$)	Reference
NiCoP/NF-PECVD	80	62	69.8	This work
NiCoP/NF-CVD	114	96	40.5	This work
NiCoP/NF	96	63	12.8	[52]
NiCoP/CNF/NF	80	62	42.7	[52]
Ni_2P/Ni/NF	98	72	27	[53]
NiCo-LDH/NF	162	141	60.9	[54]
Ni_2P/NiCoP@NCCs	116	79	--	[47]
Ni_2P/NiCoP@NHCCs	168	89	--	[47]
Ni-Co-P-300	150	60.6	--	[55]
NiCoP	124	42	28.5	[56]

4. CONCLUSIONS

In summary, a NF precursor was prepared by a hydrothermal preparation and then phosphorylated by PECVD; thus, NiCoP/NF nanoarrays were successfully grown in situ on the NF, and its high performance for electrocatalytic HER was proven. The NiCoP/NF prepared by the PECVD method has the characteristics of a rod-shaped nanoarray. The inherent structure and composition can effectively improve the electrochemical specific surface area of the material. Moreover, PECVD causes more defects to be formed on the surface of the material while moving gas molecules. This phenomenon will help increase the exposure of active sites and improve electrochemical performance. NiCoP/NF shows excellent electrocatalytic activity and excellent long-term stability to the HER in 1.0 M KOH and 0.5 M H_2SO_4. Compared with previously reported Ni-based nonnoble metal catalysts, its electrocatalytic performance is better than that of most nickel-based phosphide electrocatalysts[46-56]. This experiment will help design and prepare HER catalysts with anion-rich metal phosphide on their surfaces to achieve efficient hydrogen evolution from electrolyzing water.

ACKNOWLEDGMENTS
This work was supported by the Technology Development Fund of Jilin Province, China (20170204015SF) and the Science and Technology Project (SGTYHI/18-JS-206) of the Jilin Electric Power Research Institute Co., Ltd.

References

1. Y. Bai, H. Zhang, X. Li, L. Liu, H. Xu, H. Qiu, Y. Wang, *Nanoscale*, 7 (2015) 1446.
2. L. Zhang, D. Liu, S. Hao, L. Xie, F. Qu, G. Du, A.M. Asiri, X. Sun, *Chemistryselect*, 2 (2017) 3401.
3. M.H. Hansen, L.-A. Stern, L. Feng, J. Rossmeisl, X. Hu, *Physical Chemistry Chemical Physics*, 17 (2015) 10823.
4. Y. Pan, Y. Chen, Y. Lin, P. Cui, K. Sun, Y. Liu, C. Liu, *Journal of Materials Chemistry A*, 4 (2016) 14675.
5. Y. Pan, Y. Liu, J. Zhao, K. Yang, J. Liang, D. Liu, W. Hu, D. Liu, Y. Liu, C. Liu, *Journal of Materials Chemistry A*, 3 (2015) 1656.
6. J. Wang, L. Ji, Z. Chen, *ACS Catalysis*, 6 (2016) 6987.
7. S.L. Maslovara, D.V. Anicijevic, M.L. Kijevcanin, I.R. Radovic, V.M. Nikolic, P.Z. Lausevic, M.P.M. Kaninski, *International Journal of Hydrogen Energy*, 42 (2017) 5072.
8. D.I.M. Oertel, D.-I.J. Schmitz, D.-I.W. Weirich, c.i.D. Jendryssek-Neumann, P.D.r.n.R. Schulten, *Chemical Engineering and Technology*, 10 (1987) 248.
9. S.A. Chattanathan, S. Adhikari, N. Abdoulmoumine, *Renewable & Sustainable Energy Reviews*, 16 (2012) 2366.
10. R. Mardosaite, E. Valatka, *International Journal of Electrochemical Science*, 14 (2019) 387.
11. E.J. Popczun, J.R. McKone, C.G. Read, A.J. Biacchi, A.M. Wiltrout, N.S. Lewis, R.E. Schaak, *Journal of the American Chemical Society*, 135 (2013) 9267.
12. Z. Xing, Q. Li, D. Wang, X. Yang, X. Sun, *Electrochimica Acta*, 191 (2016) 841.
13. Q. Yu, X. Xiong, J. He, Y. Zuo, Y. Chen, C. Wang, *Environmental Science and Pollution Research*, 26 (2019) 26797.
14. S. Li, X. Liu, Y. Yuan, Z. Yan, Y. Liao, *Sheng Wu Gong Cheng Xue Bao = Chinese Journal of Biotechnology*, 24 (2008) 933.
15. Q. Han, J.S. Chen, K.R. Liu, X.J. Wei, *Journal of Alloys and Compounds*, 468 (2009) 333.
16. Z. Wang, G.F. Naterer, *International Journal of Hydrogen Energy*, 39 (2014) 14227.
17. L. Shi, C. Ling, Y. Ouyang, J. Wang, *Nanoscale*, 9 (2017) 533.
18. X. Zhang, C. Si, X. Guo, R. Kong, F. Qu, *Journal of Materials Chemistry* A, 5 (2017) 17211.
19. Y.T. Yao Huiying, X. Huang, J. Zhu, Q. Li, W. Xu, L.F. Chi, *Chinese Journal of Applied Chemistry*, 35 (2018) 328.
20. Y. Jiao, Y. Zheng, M. Jaroniec, S.Z. Qiao, *Chemical Society Reviews*, 44 (2015) 2060.
21. H.A. Gasteiger, S.S. Kocha, B. Sompalli, F.T. Wagner, *Applied Catalysis B Environmental*, 56 (2005) 9.
22. X.X. Zou, Y. Zhang, *Chem. Soc. Rev.*, 44 (2015) 5148.
23. M.P. Ruiz, J. Mijnders, R. Tweehuysen, L. Warnet, M. van Drongelen, S.R.A. Kersten, J.P. Lange, *ChemSusChem*, 12 (2019) 4395.
24. Q. Xiong, X. Zhang, H.J. Wang, G.Q. Liu, G.Z. Wang, H.M. Zhang, H.J. Zhao, *Chemical Communications*, 54 (2018) 3859.
25. J.L. Zheng, W. Zhou, Y.R. Ma, W. Cao, C.B. Wang, L. Guo, *Chemical Communications*, 51 (2015) 12863.
26. L.J. Zhang, G.R. Wang, Z.L. Jin, *New Journal of Chemistry*, 43 (2019) 6411.
27. K. Ojha, S. Saha, S.Banerjee, A.K. Ganguli, *ACS Applied Materials & Interfaces*, 9 (2017) 19455.
28. H.J. Yan, Y. Xie, Y.Q. Jiao, A.P. Wu, C.G. Tian, X.M. Zhang, L. Wang, H.G. Fu, *Advanced Materials*, 30 (2017) 1704156.
29. C. Du, L. Yang, F.L. Yang, G.Z. Cheng, W. Luo, *ACS Catalysis,* 7 (2017) 4131.
30. Y.J. Li, H. C. Zhang, M. Jiang, Y. Kuang, X.M. Sun, X. Duan, *Nano Research*, 9 (2016) 2251.
31. P. Jiang, Q. Liu, X.P. Sun, *Nanoscale*, 6 (2014) 13440.
32. Y. Pei, Y. Yang, F.F. Zhang, P. Dong, R. Baines, Y.C. Ge, H. Chu, P.M. Ajayan, J.F. Shen, M.X. Ye,

ACS Applied Materials & Interfaces, 9 (2017) 31887.
33. P.Y. Wang, Z.H. Pu, Y.H. Li, L. Wu, Z.K. Tu, M. Jiang, Z.K. Kou, I.S. Arniinu, S.C. Mu, *ACS Applied Materials & Interfaces*,9 (2017) 26001.
34. Y.Q. Gong, Z.F. Xu, H.L. Pan, Y. Lin, Z. Yang, J.L. Wang, *Journal of Materials Chemistry A,* 6 (2018) 12506.
35. J.G. Wang, W. Hua, M.Y. Li, H.Y. Liu, M.H. Shao, B.Q. Wei, *ACS Applied Materials&Interfaces*, 10b(2018) 41237.
36. J.Z. Li, G.D. Wei, Y.K. Zhu, Y.L. Xi, X.X. Pan, Y. Ji, I.V. Zatovsky, W. Han, *Journal of Materials Chemistry A*, 5 (2017) 14828.
37. Q. Fu, T. Wu, G. Fu, T.L. Gao, J.C. Han, T. Yao, Y.M. Zhang, W.W. Zhong, X.J. Wang, B. Song, *ACS Energy Letters*, 3v(2018)v1744.
38. A.J. Wang, M.L. Qin, J. Guan, L. Wang, H.C. Guo, X. Li, Y. Wang, R. Prins, Y.K. Hu, *Angewandte Chemie*, 47 (2008) 6052.
39. H.F. Liang, A.N. Gandi, D.H. Anjum, X.B. Wang, U. Schwingenschlogl, H.N. Alshareef, *Nano Letters*, 16 (2016) 7718.
40. J. Liang, Y. Zheng, J. Chen, J. Liu, D. Hulicova-Jurcakova, M. Jaroniec, S.Z. Qiao, *Angewandte Chemie International Edition*, 51 (2012) 3892.
41. M.C. Biesinger, B.P. Payne, A.P. Grosvenor, L.W.M. Lau, A.R. Gerson, R.S. Smart, *Applied Surface Science*, 257 (2011) 2717.
42. A.P. Grosvenor, M.C. Biesinger, R.S.C. Smart, N.S. McIntire, *Surface Science*, 600 (2006) 1771.
43. H.W. Huang, C. Yu, C.T. Zhao, X.T. Han, J. Yang, Z.B. Liu, S.F. Li, M.D. Zhang, J.S. Qiu, *Nano Energy*, 34 (2017) 472.
44. A.W. Burns, K.A. Layman, D.H. Bale, M.E. Bussell, *Applied Catalysis A General*, 343 (2008) 68.
45. P.E.R. Blanchard, A.P. Grosvenor, R.G. Cavell, A. Mar, *Chemistry of Materials*, 20 (2008) 7081.
46. K.W. Wang, X.L. She, S. Chen, H.L. Liu, D.H. Li, Y. Wang, H.W. Zhang, D.J. Yang, X.D. Yao, *Journal of Materials Chemistry A*, 6 (2018) 5560.
47. L. Han, T.W. Yu, W. Lei, W.W. Liu, K. Feng, Y.L. Ding, G.P. Jiang, P. Xu, Z.W. Chen, *Journal of Materials Chemistry A*, 5 (2017) 16568.
48. M.J. Liu, J.H. Li, *ACS Applied Materials & Interfaces*, 8 (2015) 2158.
49. C. Wu, Y.J. Yang, D. Dong, Y.H. Zhang, J.H. Li, *Small*, 13 (2017) 1602873.
50. L.T. Yan, P.C. Dai, Y. Wang, X. Gu, L.J. Li, L. Cao, X.B. Zhao,*ACS applied materials & interfaces*, 9 (2017) 11642.
51. X.P. Zhang, Y.J. Han, L. Huang, S.J. Dong, *ChemSusChem*, 9 (2016) 3049.
52. J. Wu, X.B. Ge, Z.H. Li, D. Cao, J.Y. Xiao, *Electrochimica Acta*, 252 (2017) 101.
53. B. You, N. Jiang, M. Sheng,W. Bhushan, Y. Sun, *ACS Catalysis*, 6 (2015) 714.
54. W.J. Liu, J. Bao, M.L. Guan, Y. Zhao, J.B. Lian, J.X. Qiu, L. Xu, Y.P. Huang, J. Qian, H. Li, *Dalton Transactions*, 46 (2017) 8372.
55. Y. Feng, X.Y. Yu, U. Paik, *Chemical Communications*, 52 (2016) 1633.
56. Y.P. Li, J.D. Liu, C. Chen, X.H. Zhang, J.H. Chen, ACS Applied Materials & Interfaces, 9 (2017) 5982.